Quantum turnstile operation of single-molecule magnets

2015 New J. Phys. 17 083020

(http://iopscience.iop.org/1367-2630/17/8/083020)

New Journal of Physics
The open access journal at the forefront of physics

Deutsche Physikalische Gesellschaft DPG
IOP Institute of Physics

Published in partnership with: Deutsche Physikalische Gesellschaft and the Institute of Physics

OPEN ACCESS

RECEIVED
8 April 2015

REVISED
16 June 2015

ACCEPTED FOR PUBLICATION
2 July 2015

PUBLISHED
11 August 2015

PAPER

Quantum turnstile operation of single-molecule magnets

V Moldoveanu[1], I V Dinu[1], B Tanatar[2] and C P Moca[3,4]

[1] National Institute of Materials Physics, PO Box MG-7, Bucharest-Magurele, Romania
[2] Department of Physics, Bilkent University, Bilkent, 06800 Ankara, Turkey
[3] BME-MTA Exotic Quantum Phase Group, Institute of Physics, Budapest University of Technology and Economics, H-1521 Budapest, Hungary
[4] Department of Physics, University of Oradea, 410087, Oradea, Romania

Keywords: single-molecule magnets, quantum turnstile, magnetic qubits

Abstract

The time-dependent transport through single-molecule magnets coupled to magnetic or non-magnetic electrodes is studied in the framework of the generalized master equation method. We investigate the transient regime induced by the periodic switching of the source and drain contacts. If the electrodes have opposite magnetizations the quantum turnstile operation allows the stepwise writing of intermediate excited states. In turn, the transient currents provide a way to read these states. Within our approach we take into account both the uniaxial and transverse anisotropy. The latter may induce additional quantum tunneling processes which affect the efficiency of the proposed read-and-write scheme. An equally weighted mixture of molecular spin states can be prepared if one of the electrodes is ferromagnetic.

1. Introduction

Single-molecule magnets (SMMs) are foreseen as building blocks of organic spintronic devices [1, 2]. Such systems generally behave as magnetic cores with a large localized spin and display slow relaxation of magnetization at low temperature mostly due to the presence of the anisotropy-induced magnetic barrier [3]. Similar to quantum dot physics, two-terminal steady-state transport measurements performed on SMMs revealed charging effects such as Coulomb blockade, sequential tunneling or negative differential conductance [4, 5]. In the spin sector, Kondo related features were observed experimentally [6–9] and investigated theoretically [10, 11]. The exchange interaction between the local molecular moment and the delocalized spins tunneling through the molecular orbital might be exploited to control the quantum state of the local moment, i.e. to 'write' and 'read' its quantum state [12].

On the experimental side, various techniques [13] are currently used to attach the orbitals (ligands) surrounding the molecular magnetic core to the source and drain probes. Unlike standard transport setups used in quantum dot devices, molecular electronics requires more careful handling of the contact regions. The difficult task of isolating a single molecule between source and drain electrodes is nowadays realized by using more advanced methods as electromigration, mechanically controlled break junctions [14] or spin polarized STM [15]. Recently several groups pushed these techniques even further and reported controlled time-dependent transport measurements for such SMMs when the contacts were switched on and off by varying the substrate-STM tip spacing [16, 17] or by bending break junctions [18], and transient currents arising when a molecular tail couples to an STM tip have been recorded [19]. SMMs have also been integrated into carbon nanotube transistors to serve as detectors for the nanomechanical motion due to the strong spin–phonon coupling [20, 21]. In two cornerstone experiments Vincent *et al* [22] and Thiele *et al* [23] detected the nuclear spin of a single Tb^{3+} ion embedded in a SMM together with the Rabi oscillations.

These promising experiments motivated us to investigate the transient transport properties of SMMs, with special emphasis on the regime when the couplings to the source/drain electrodes are switched on and off periodically. The transport regime we are interested in is similar to the so-called turnstile pumping setup which represents a long-standing [24] asset of pumping or pump-and-probe experiments with quantum dots [25].

Along this periodic pumping, the source and drain tunneling barriers open and close consecutively, such that a single electron is transmitted across the sample; details on the turnstile operation will be presented in section 3. To our best knowledge the transient and the turnstile regimes have not been theoretically investigated so far in the context of transport across SMMs.

On the theoretical side the magnetic interactions in SMMs are described by effective giant spin Hamiltonians [3], mostly because of the large value of the localized magnetic moment. Using this description, in [26] the authors investigated the role of relaxation on inelastic charge and spin transport across a SMM weakly coupled to metallic gates. In [27] transport across a SMM coupled to two ferromagnetic leads was investigated and it was found that the spin current across the SMM can reverse the localized spin if the leads have opposite spin polarizations. Memristive [28] and thermoelectric [29] properties of SMMs were also investigated. All these studies convey a similar message: the current can induce magnetic switching of the localized magnetic moment if the applied bias voltage exceeds the gap between the ground and excited states.

In the absence of transverse anisotropy the effect of quantum tunneling of magnetization (QTM) is negligible and the full magnetic switching requires the *transient* occupation of all excited (intermediate) states with magnetic quantum numbers in the range $[-S,\ S]$. When present, the QTM might leave its fingerprint on the transport properties at resonant values of an applied magnetic field [30].

A complementary approach to transport properties of SMMs relies on density functional theory (DFT) [31, 32]. In the DFT approach the molecular structure and the contact regions are carefully taken into account, while the many-body correlations within the SMM are accounted for within various approximations. A detailed *ab initio* Hubbard many-body model for molecular magnets has been recently implemented [33] and allows the calculation of magnetic interactions.

In the present work we investigate transient transport and turnstile pumping across a SMM embedded between magnetic and non-magnetic electrodes. As we are interested in the time-dependent evolution of the currents and the accumulation of the charge and spin on the SMM we rely our investigation on the generalized master equation (GME) technique [34, 35]. Let us stress that, to capture the turnstile regime, one has to go beyond the steady-state rate-equation approach. We find that by setting the SMM in the quantum turnstile (QT) configuration with ferromagnetic leads one can address two new issues which are relevant for the use of molecular states as magnetic qubits: (i) the one-by-one all-electrical writing and reading of excited molecular states with spin $S-1$,.., $-S+1$ (S being the molecular spin of the initial ground state) and (ii) the controlled preparation of statistical mixtures of such intermediate states. So far, the *stepwise* magnetic switching protocols for excited molecular states that we propose here have not been investigated. In fact, previous studies (see e.g. [26, 27]) were focused only on investigating the full magnetic switching. The second issue was partially addressed by Tejeda *et al* [36] some time ago. Their proposal concerns the preparation of equal weight superposition of states (e.g. $|\psi\rangle = 1/\sqrt{2}\ (|S\rangle + |S-1\rangle)$) using at least two molecular clusters embedded in micro-SQUIDs.

The rest of the paper is organized as follows. In section 2 we present the theoretical framework by introducing the model Hamiltonian and giving a summary of the GME method. Section 3 presents the main results of our work while in section 4 we give the conclusions.

2. Theoretical framework

2.1. Model Hamiltonian

The setup that we consider here consists of an SMM coupled to two external electrodes (see the sketch in figure 1). We investigate time-dependent transport in the sequential tunneling regime, in which the electrons tunnel one by one from the left (source) electrode to the unoccupied molecular orbitals of SMM and then escape to the right (drain) electrode. In the present work we neglect all other possible transport mechanisms, such as the cotunneling processes which are responsible for the Kondo effect [10].

The model Hamiltonian contains several terms describing the SMM itself (H_M), the left (H_L) and right (H_R) electrodes and the time-dependent tunneling part H_T:

$$H(t) = H_M + H_L + H_R + H_T(t). \tag{1}$$

In general, SMMs are characterized by a large spin $S > 1/2$. They do also present transverse anisotropy and an easy axis of magnetization [3]. Assuming that the relevant contribution to the transport comes only from the lowest unoccupied molecular orbital (LUMO) the SMM can be modeled by an effective, minimal Hamiltonian [26, 27] of the form:

$$H_M = \varepsilon\ \hat{n} + U\hat{n}_\uparrow\hat{n}_\downarrow - J\hat{\mathbf{s}}\cdot\hat{\mathbf{S}} - D\hat{S}_z^{\,2} + E\left(\hat{S}_x^{\,2} - \hat{S}_y^{\,2}\right) - g\mu_B B\hat{S}_z^{\,t}. \tag{2}$$

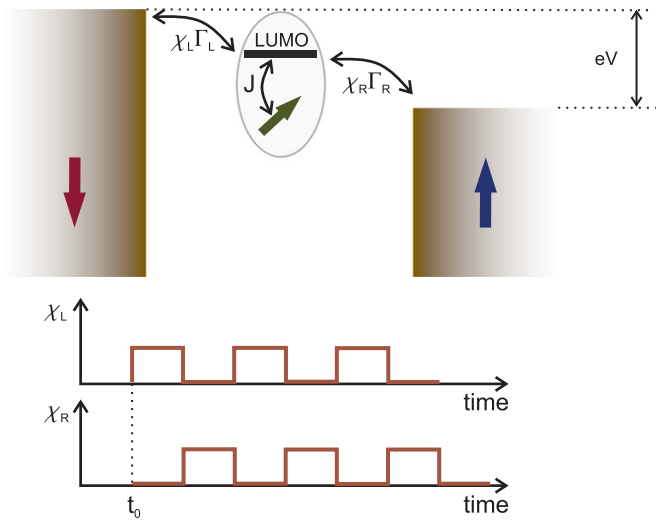

Figure 1. A sketch of the SMM coupled to source and drain electrodes via time-dependent tunneling barriers. The tunneling amplitudes are controlled by the switching functions χ_L and χ_R. The turnstile operation consists of turning the contacts on and off periodically. Note that the left contact opens first, for the charging sequence, while the right contact couples later for the discharge/depletion sequence. The chemical potentials of the leads are chosen such that $\mu_L > \mu_R$; the bias $eV = \mu_L - \mu_R$. The value t_0 is some initial time. The leads are spin polarized in the so-called antiparallel (AP) configuration.

In its simplest form the LUMO orbital consists of a single spinful interacting level with energy ε, on-site Coulomb energy U and occupation $\hat{n} = \hat{n}_\uparrow + \hat{n}_\downarrow$, and is coupled to the localized spin $\hat{\mathbf{S}}$ through an exchange interaction with a coupling strength J. The fourth and the fifth terms in equation (2) describe the easy-axis and transverse anisotropy with the corresponding constants denoted by D and E. For certain molecules [38] $E \ll D$ but this is not always true, as E can grow up to $D/3$ in other situations [3]. In the presence of an external magnetic field B pointing in the z-direction, a Zeeman term is supplemented in equation (2), with g and μ_B being the gyromagnetic factor and the Bohr magneton, respectively. In view of further discussions we single out the transverse anisotropy term and write H_M in equation (2) as

$$H_M = H_M^0 + E\left(\hat{S}_x^{\,2} - \hat{S}_y^{\,2}\right). \tag{3}$$

The reason behind this separation is that, contrary to H_M, H_M^0 has an extra abelian $U(1)$ symmetry generated by the z-component of the total spin $\hat{S}_z^{\,t} = \hat{S}_z + \hat{s}_z$. Consequently, the eigenstates of H_M^0 can be organized according to the eigenvalues m of $\hat{S}_z^{\,t}$.[5] On the other hand the transverse anisotropy term does not commute with $\hat{S}_z^{\,t}$ and needs to be treated separately. We shall discuss in more detail the eigenstates of H_M^0 in section 2.2.

The source and drain electrodes are modeled as spin-polarized one-dimensional discrete chains which in the momentum space representation are described by the Hamiltonians:

$$H_\alpha = \sum_\sigma \int_0^\pi \mathrm{d}q_\alpha\ \varepsilon_{q_\alpha\sigma}\ a^\dagger_{q_\alpha\sigma} a_{q_\alpha\sigma}, \qquad \alpha = \{L, R\}. \tag{4}$$

Both leads present an energy dispersion law of the form $\varepsilon_{q\sigma} = 2\tau\ \cos q + \Delta_\sigma$, with τ the effective hopping between the nearest neighbor sites in the leads and Δ_σ a rigid-band spin splitting that describes the polarization of the leads. In equation (4) $a^\dagger_{q_\alpha\sigma}$ creates an electron with momentum q and spin σ in the lead $\alpha = \{L, R\}$.

The last term in equation (1) describes the hybridization of the SMM with the contacts

$$H_T(t) = \sum_{\alpha=L,R}\sum_\sigma \int_0^\pi \mathrm{d}q_\alpha \chi_\alpha(t)\left(V_\sigma^\alpha a_\sigma^\dagger a_{q_\alpha\sigma} + h.c\right), \tag{5}$$

where $a_\sigma^\dagger$ creates an electron with spin σ on the LUMO orbital and V_σ^α is the hopping amplitude of a tunneling process between the LUMO and the majority ($\sigma = +$) and minority ($\sigma = -$) electron states in the lead α. The coupling of the SMM to the contacts in the case of collinear magnetic configuration, and in the absence of the switching protocol ($\chi_\alpha(t) = 1$), is described by $\Gamma_\sigma^\alpha = 2\pi|V_\sigma^\alpha|^2\ \varrho_{\alpha\sigma}(0)$, where $\varrho_{\alpha\sigma}(0)$ is the spin density of states at the Fermi surface for electrons in lead α.

In view of further investigations we allow tunable spin polarizations in the leads and define $P^\alpha := (\Gamma_+^\alpha - \Gamma_-^\alpha)/(\Gamma_+^\alpha + \Gamma_-^\alpha)$.

[5] It can be easily shown that $[H_M, \hat{S}_z^{\,t}] = 0$ if $E = 0$.

Note that the Hamiltonian $H_T(t)$ contains two time-dependent dimensionless functions $\chi_\alpha(t)$ $(\alpha = L, R)$ which simulate the switching of the contacts between the molecule and the leads. As we are interested in the turnstile pumping it is enough to consider them simply as rectangular periodic pulses (see figure 1).

2.2. Energy eigenstates

In this section we discuss the energy spectrum and the organization of the eigenstates of the SMM Hamiltonian H_M introduced in equation (2). We shall start by discussing first the spectrum of H_M^0. When $J = 0$, the LUMO orbital gets decoupled from the local spin and the Hamiltonian H_M^0 has three $U(1)$ symmetries generated by the local charge Q accumulated on the LUMO and by the z-components of the LUMO and local spins, $\hat{s}_z$ and $\hat{S}_z$. Consequently, $\{Q, \hat{s}_z, \hat{S}_z\}$ provides the quantum numbers according to which the multiplets of the Hamiltonian are classified. Notice that this low symmetry classification is valid for finite magnetic fields. When $B = 0$, the Hamiltonian H_M^0 has a much higher symmetry, i.e. $U_Q(1) \times SU_{\hat{\mathbf{s}}}(2) \times SU_{\hat{\mathbf{S}}}(2)$ in the charge and spin sectors, but this situation shall not be discussed here, as we always assume a finite magnetic field. In the case we consider here, the classification of the states is rather trivial and we can simply denote the eigenstates as follows: $|0, 0, S_z\rangle$, $|1, \uparrow, S_z\rangle$, $|1, \downarrow, S_z\rangle$, and $|2, 0, S_z\rangle$, with $S_z = -S, -S+1, .., S$. In the presence of Coulomb interaction the double occupied states $|2, 0, S_z\rangle$ have an energy of the order $\sim U$, which is the largest energy scale in the problem, and in view of the discussion that follows, shall not contribute to transport. Therefore, to simplify the notations, it is enough to relabel the states and keep track of the $\hat{s}_z$ and $\hat{S}_z$ quantum numbers. In this new notation we have $|0, 0, S_z\rangle \to |0, S_z\rangle$ and $|1, \sigma, S_z\rangle \to |\sigma, S_z\rangle$.

A finite exchange coupling J breaks the three $U(1)$ symmetries down to $U_Q(1) \times U_{\hat{S}_z^t}(1)$ generated by LUMO charge Q and the z-component of the total spin $\hat{S}_z^t$. Still, the Hamiltonian H_M^0 can be diagonalized exactly and the states constructed in an analytical fashion in terms of the states introduced previously for $J = 0$, by using the Clebsch–Gordan construction [26]. Now the new states $|Q, m\rangle$ shall be classified by the molecular charge Q, and by the z-component of the total spin, m.

For $m \in [-S + 1/2, S - 1/2]$ the single-particle states $(Q = 1)$ are given by:

$$|1, m\rangle^{\pm} = C^{\pm}_{m\downarrow} |\downarrow, m + 1/2\rangle + C^{\pm}_{m\uparrow} |\uparrow, m - 1/2\rangle, \tag{6}$$

and their associated eigenvalues $\mathcal{E}^{\pm}_{1,m}$ read as:

$$\mathcal{E}^{\pm}_{1,m} = \epsilon - g\mu_B Bm + \frac{J}{4} - D\left(m^2 + \frac{1}{4}\right) \pm \Delta\mathcal{E}(m), \tag{7}$$

where $\Delta\mathcal{E}(m) = [D(D - J)m^2 + (J/4)^2(2S + 1)^2]^{1/2}$. The coefficients $C^{\pm}_{m\sigma}$ in equation (6) are simply the Clebsch–Gordan coefficients. The states $|0, S_z\rangle$ are not affected by the exchange coupling and one has $|0, m\rangle = |0, S_z\rangle$. The corresponding eigenvalue is simply $\mathcal{E}_{0,m} = -DS_z^2 - g\mu_B BS_z$. The remaining $Q = 1$ states are $|1, -S - 1/2\rangle$ and $|1, S + 1/2\rangle$. For a vanishing magnetic field, $B = 0$, the states associated to $\pm m$ are degenerate and one has

$$\mathcal{E}^{\pm}_{1,m}(B = 0) = \mathcal{E}^{\pm}_{1,-m}(B = 0), \tag{8}$$

$$\mathcal{E}_{0,m}(B = 0) = \mathcal{E}_{0,-m}(B = 0). \tag{9}$$

So far we have discussed how to construct the states and how to compute the energy spectrum for H_M^0. In the rest of this paragraph we shall address the role of the transverse anisotropy term. The transverse anisotropy term $\sim(\hat{S}_x^2 - \hat{S}_y^2) \sim (\hat{S}_+^2 + \hat{S}_-^2)$ does not commute with $\hat{S}_z^t$ and induces transitions [3] between the states of H_M^0 with the selection rule $|m - m'| = 2$.

As the molecular charge is a good quantum number even in the presence of the transverse anisotropy, the eigenstates of the total molecular Hamiltonian H_M can be classified by the molecular charge Q only. We shall label them $|\varphi_{Q,\nu}\rangle$, where $Q = \{0, 1\}$ (states with molecular charge $Q = 2$ are disregarded) while ν is an internal label that indexes the states within a multiplet. In the presence of the transverse anisotropy E, the 'empty' molecular states (EMS) can be written as:

$$|\varphi_{0,\nu}\rangle = \sum_m c_{\nu,m} |0, m\rangle, \quad \nu = 1, .., 2S + 1, \tag{10}$$

with m running over all allowed values in the range $[-S, S]$. For half-integer S and a small magnetic field, the transverse anisotropy plays a minor role in the mixing of the states $|\varphi_{0,\nu}\rangle$, as the transition amplitudes between the empty molecular states $\{|0, m\rangle\}$ are negligible (see also the discussion following figure 2).

In contrast, the transverse anisotropy couples the degenerate, one-particle states $(Q = 1)$ with opposite m's. The strongest mixing is expected for the pairs $|1, 1\rangle^{\pm}$ and $|1, -1\rangle^{\pm}$ as the off-diagonal matrix element ${}^{\pm}\langle 1, 1|H_M|1, -1\rangle^{\pm}$ is linear in E. Higher order mixing effects become important as the ratio E/D increases and one can generally write:

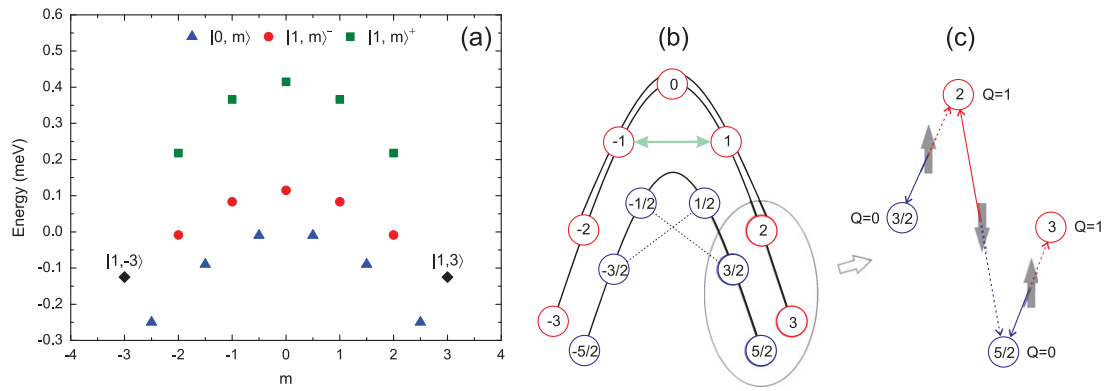

Figure 2. (a) The energy levels for a SMM of spin $S = 5/2$ as function of the total magnetic quantum number m. The two-particle sector is not included as the corresponding states are outside the selected bias window. Other parameters are: ϵ=0.25 meV, J=0.1 meV, U=1 meV, D=0.04 meV, $g\mu_B B = 0$ and E=0. (b) The transverse anisotropy E induces mixing of degenerate or nearly degenerate states with $m = 1$ and $m = -1$ (indicated by the double arrow). There is no significant quantum tunneling of magnetization between the states $|0, \mp 1/2\rangle$ and $|0, \pm 3/2\rangle$ (indicated by the dashed lines). The numbers in the circles are the total magnetic quantum numbers m. (c) Tunneling processes connecting the lowest four states of the SMM via back-and-forth tunneling with the leads. These states are also involved in the first turnstile cycle; see the discussion in the text.

$$|\varphi_{1,\nu}\rangle = \sum_m \sum_s c^s_{\nu,m} |1, m\rangle^s, \quad \nu = 1,..,2(2S+1). \tag{11}$$

The eigenvalues $E_{Q,\nu}$ of H_M and the coefficients in equations (10) and (11) can be found only by numerical diagonalization. More details on the spectral properties and state mixing will be given in section 3.

Finally, we write down the matrix elements of the tunneling Hamiltonian H_T with respect to the eigenstates of H^0_M and derive the selection rules for molecular transitions due to electronic back-and-forth processes namely ($\lambda_\uparrow = 1, \lambda_\downarrow = -1$):

$$^{\pm}\langle 1, m| a^\dagger_\sigma |0, m'\rangle = C^{\pm}_{m\sigma}\delta_{m,m'+\lambda_\sigma/2}. \tag{12}$$

This equation describes the tunneling of one electron with spin σ on the SMM orbital, when the number of electrons in the molecule increases by one while the *total* magnetic quantum number m changes by $\pm 1/2$.

2.3. Generalized master equation approach

The GME approach which we use to investigate the time-dependent transport relies on the partitioning approach [37]. More precisely, transient currents develop in the source and drain electrodes as they are contacted to the molecule at some initial instant. The leads are viewed as non-interacting particle reservoirs with chemical potentials μ_α ($\alpha = L, R$), and at equilibrium described by the Hamiltonian (4). This setting is suitable for perturbative calculations with respect to the lead-molecule couplings $\Gamma^\alpha_\pm$, and allows us to compute transient currents in the presence of time-dependent modulation of the contacts, as in the turnstile regime.

The GME method essentially provides the SMM reduced density operator (RDO) ρ defined as the partial trace over the leads' degrees of freedom $\rho(t) = \mathrm{Tr}_{\mathcal{F}_{\rm el}}\{W(t)\}$. Here $W(t)$ is the density operator of the whole structure which solves the Liouville–von Neumann equation $i\hbar\dot{W}(t) = [H(t), W(t)]$, and the trace is over $\mathcal{F}_{\rm el}$, which is the Fock space of the non-interacting electronic reservoirs. In the sequential tunneling regime considered here the master equation takes a rather compact form (for a full derivation see [34]):

$$\frac{\mathrm{d}\rho(t)}{\mathrm{d}t} = -\frac{i}{\hbar}\Big[H_M, \rho(t)\Big] - \frac{1}{\hbar^2}\mathrm{Tr}_{\mathcal{F}_{\rm el}}\Big\{\mathcal{D}_t[\rho]\Big\}, \tag{13}$$

$$\mathcal{D}_t[\rho] = \left[H_T(t), \int_0^t \mathrm{d}s U_{t-s}\Big[H_T(s), \rho(s)\rho_{\rm el}\Big]U^*_{t-s}\right], \tag{14}$$

where we introduced the 'free' evolution operator of the disconnected system $U_t = \mathrm{e}^{-\mathrm{i}(H_M+H_L+H_R)t/\hbar}$ and the equilibrium distribution of the leads $\rho_{\rm el}$.[6] The dissipative operator $\mathcal{D}_t$ collects all sequential tunneling processes from the switching instant $t_0 = 0$ to the current time t. We solve numerically equation (13) with respect to the fully interacting states of H_M and obtain the populations associated to a given state $|\varphi_{Q,\nu}\rangle$ as

[6] For non-interacting leads $\rho_{\rm el}$ is defined through the identity $\mathrm{Tr}_{\mathcal{F}_L}\{\rho_{\rm el} a^\dagger_{q_\alpha\sigma} a_{q_\beta\sigma}\} = \delta_{\sigma\sigma'}\delta_{\alpha\beta} f_\alpha(\epsilon_{q_\alpha})$, where $f_\alpha(\epsilon_{q_\alpha})$ is the Fermi function associated to the lead α.

$$P_{Q,\nu}(t) = \langle\varphi_{Q,\nu}|\,\rho(t)|\varphi_{Q,\nu}\rangle. \tag{15}$$

Once $\rho(t)$ is known one can calculate the average values of molecular observables by performing a trace over the Fock space $\mathcal{F}_M$ of the molecule. For instance, the total charge accumulated on the orbital involved in transport is given by

$$Q(t) = e\mathrm{Tr}_{\mathcal{F}_M}\{\rho(t)\hat{N}\}, \tag{16}$$

where the total electronic occupation $\hat{N} = \hat{n}_\uparrow + \hat{n}_\downarrow$ and e is the electron charge. The continuity equation then becomes [35]

$$J_L(t) - J_R(t) = \sum_Q \sum_{\nu_Q} \langle\varphi_{Q,\nu_Q}|\,\dot{\rho}(t)|\varphi_{Q,\nu_Q}\rangle, \tag{17}$$

where ν_Q is the set of states with charge Q. By inserting H_T into the double commutator $\mathcal{D}_t$ given in equation (14) one identifies J_L and J_R from the RHS of equation (17). It is straightforward to show that the 'empty' molecular states $|\varphi_{0,\nu}\rangle$ do not contribute to the currents. Similarly, one can calculate the total spin $\langle S_z^t\rangle = \mathrm{Tr}_{\mathcal{F}_M}\{\rho(t)\hat{S}_z^t\}$ as well as the spin currents. In this work the relaxation of the excited molecular states via phonon emission is not considered. This is a good approximation as long as the timescale on which the quantum turnstile operates is much smaller than the relaxation time which is of order of 10^{-6} s (see e.g [39, 40]). In fact previous studies [41] reported that the current-induced magnetic switching is stable against intrinsic spin–relaxation processes.

3. Results and discussion

3.1. The transport configuration and tunneling processes

The numerical simulations were performed for molecules with spin $S = 5/2$ but our conclusions remain valid for larger half-integer values of S. For reasons that will become clear below, in this work we restrict ourselves to SMMs with small transverse anisotropy, that is $E \ll D \ll J$ (in fact we allow a maximum ratio $E/D = 1/25$ at fixed easy-axis anisotropy constant D). We shall investigate two spin configurations for the leads. In the so-called antiparallel (AP) configuration the left lead carries only spin-down electrons and the right lead is spin-up polarized. For the second configuration the left lead is non-magnetic (i.e. $P^L = 0$) and the right lead remains ferromagnetic. We label this configuration as normal-ferromagnetic (NF).

The chemical potential of the leads $\mu_{L,R}$ are set such that only the states $|\varphi_{0,\nu}\rangle$ and $|\varphi_{1,\nu}\rangle$ contribute to the tunneling processes, while double occupied states, $|\varphi_{2,\nu}\rangle$, have much higher energies, $E_{2,\nu} > \mu_L$, and do not contribute to transport.

Let us first discuss the energy spectrum and the relevant lead-molecule tunneling processes *in the absence of transverse anisotropy*. In the following discussion we shall use the basis $\{|Q,\ m\rangle\}$ of $H_M^0 = H_M(E = 0)$. As we are interested in the pumping mechanism at finite transverse anisotropy E, we shall switch later to the basis $|\varphi_{Q,\nu}\rangle$ of the full H_M. In that situation, with certain modifications, a similar turnstile scenario holds. Figure 2(a) shows the energy levels of H_M^0 for a given set of parameters, and in the absence of the external magnetic field. Figure 2(b) schematically shows the charge $Q = 1$ (integer m's) and $Q = 0$ (half integer m's) branches of the spectrum; in view of further discussion the double arrow and the dotted lines mark some of the quantum tunneling of magnetization (QTM) processes induced by a nonvanishing E. The states connected by the double arrow are strongly mixed by E, while the ones connected by the dashed lines are only weakly coupled. As charge Q is conserved, it implies that direct transitions between $Q = 0$ and $Q = 1$ branches are forbidden by symmetry. This is only possible through processes involving states in the leads that do not conserve the charge. For example in figure 2(c), we show such processes (blue and red arrows). The same figure also shows how the SMM evolves from an initial 'empty' molecular state $|0,\ 5/2\rangle$ to the to the next EMS $|0,\ 3/2\rangle$ via tunneling processes.

We shall call the transitions $m \to m - 1/2$ 'forward' processes (they follow the full line arrows in figure 2(c)) as they contribute to the magnetic switching $m = 5/2 \to m = -5/2$. On the other hand the transitions $m \to m + 1/2$ compete for the total spin reversal and can be regarded as 'backward' processes (they follow the dashed lines in figure 2(c)).

Furthermore, we distinguish two types of 'forward' transitions: (i) 'absorption' of spin-down electrons from the leads, i.e. the charging of the molecular orbital along the transitions $|0,\ m\rangle \to |1,\ m - 1/2\rangle^{\pm}$ (full red arrow in figure 2(c)) and (ii) tunneling of spin-up electrons from the molecular orbital, i.e. a depletion process associated to the transitions $|1,\ m - 1/2\rangle^{\pm} \to |0,\ m - 1\rangle$ (full blue arrow). Similarly one defines charging and discharging 'backward' processes (associated with the dashed lines in figure 2(c)). We find this analysis useful as it provides hints for a write-and-read scheme of states with well-defined molecular spin $|0,\ m\rangle$ when operating the SMM in the turnstile regime. Such a protocol will be discussed in the next subsection.

3.2. The turnstile protocol

A turnstile pumping cycle entails two steps: (i) the charging of the molecular orbital from the left lead while the drain contact is closed ($\chi_L(t) \neq 0$, $\chi_R(t) = 0$) and (ii) discharging/depletion through the drain lead ($\chi_L(t) = 0$, $\chi_R(t) \neq 0$). We simulate the turnstile operation by appropriately tailoring the switching functions χ_L and χ_R in the tunneling Hamiltonian H_T.

The main idea behind the proposed operation is the following: use the charging sequences to prepare intermediate one-electron states via 'forward' tunneling from the left lead and write 'empty' molecular states $|0,\ m\rangle$ along 'forward' depletions to the right lead. To be more precise, let us discuss a single turnstile cycle at $E = 0$ in the NF configuration, starting from the initial state $|0,\ 5/2\rangle$. The associated transitions are depicted in figure 2(c). By opening the source (left) contact, the states $|1,\ 2\rangle^{\pm}$ become populated by absorbing one spin $-\downarrow$ electron (forward tunneling). In turn, if a spin$-\uparrow$ electron is absorbed then the rightmost state $|1,\ 3\rangle$ becomes activated (backward tunneling). Then, the left contact closes and the drain (right) electrode comes into play. Now, the orbital is depleted through forward tunneling $|1,\ 3\rangle \rightarrow |0,\ 5/2\rangle$ and $|1,\ 2\rangle^{\pm} \rightarrow |0,\ 3/2\rangle$, as spin$-\uparrow$ electron tunnels out into the right lead. An accurate operation would lead to the preparation of a *single* EMS or to an equally weighted mixture of EMS, but this scenario is not expected to work if the transverse anisotropy induces strong mixing of states $|0,\ m\rangle$.

In view of this analysis, let us now discuss how this picture gets modified in the presence of the transverse anisotropy. We start by describing the construction of the empty molecular states $\{|\varphi_{0,\nu}\rangle\}$. We find that if $g\mu_B B \ll D$ the mixing of 'empty' molecular states $|0,\ m\rangle$ is negligible since the QTM between the states $|0,\ \mp 1/2\rangle$ and $|0,\ \pm 3/2\rangle$ is very weak (see the dotted lines in figure 2(b)). In this case we find a one to one correspondence between $\nu \leftrightarrow m$ as for any ν in equation (10) one can find a single m such that $|\varphi_{0,\nu}\rangle \approx |0,\ m\rangle$.

This simple correspondence fails as the magnetic field approaches resonant value $g\mu_B B_{\rm res} = -D(S_z + S_z')$, and the Landau–Zenner tunneling processes between $\mathcal{E}_{0,m}$ and $\mathcal{E}_{0,m'=m\pm 2}$ become important and lead to strong mixing of the states. Such a resonant regime will not be discussed in the present work.

We now turn to $Q = 1$ states. For $B = 0$, the states $|1,\ m\rangle^{\pm}$ and $|1,\ -m\rangle^{\pm}$ in equation (11) are mixed by the transverse anisotropy term as $\mathcal{E}^{\pm}_{1,m}$ and $\mathcal{E}^{\pm}_{1,-m}$ are degenerate (see equation (8)). The mixing is indicated by the double arrow in figure 2(b). However, even a small magnetic field lifts this degeneracy and one finds a rather small mixing of the states $|1,\ m\rangle^{\pm}$ and $|1,\ -m\rangle^{\pm}$ for $E \neq 0$. Once again, for each $|\varphi_{1,\nu}\rangle$ there is a single state $|1,\ m'\rangle^{s}$ of H^0_M whose weight $|c^{s}_{\nu,m'}|^2$ in equation (11) is by far the largest one. Under these conditions the one-to-one correspondence between the index ν and the quantum number m is preserved for all states and allows us to index them as:

$$|\varphi_{1,\nu}\rangle \rightarrow |\varphi^{s}_{1,m}\rangle \approx |1,\ m\rangle^{s}, \quad |\varphi_{0,\nu}\rangle \rightarrow |\varphi_{0,m}\rangle \approx |0,\ m\rangle. \tag{18}$$

We shall close this section by noticing that although this representation works, ν will always be read as an index, and not as a quantum number. Consequently, in the $|\varphi^{s}_{1,m}\rangle$ basis the populations of the states will be denoted by $P_{|\varphi^{s}_{1,m}\rangle}$ and $P_{|\varphi_{0,m}\rangle}$.

3.3. Writing and reading the excited molecular states

We performed transport calculations starting from the initial state $|\varphi_{0,5/2}\rangle$, so the density matrix describing the system at $t = 0$ is $\rho(t = 0) = |\varphi_{0,5/2}\rangle\langle\varphi_{0,5/2}|$. As stated previously, we shall present results for small values of the ratio $E/D \sim 10^{-2}$. The evolution of the relevant populations along a *single* turnstile cycle in the normal-ferromagnetic (NF) configuration for $E/D = 1/250$ is presented in figures 3(a) and (b). The tunneling processes are similar to the ones discussed along figure 2(c) when $E = 0$. The state $|\varphi_{1,3}\rangle$ is half filled through spin-up 'backwards' tunneling whereas $P_{|\varphi^{+}_{1,2}\rangle} + P_{|\varphi^{-}_{1,2}\rangle} = 1/2$. The small imbalance population of the states $|\varphi^{\pm}_{1,2}\rangle$ is due to the finite J, while $P_{|\varphi^{+}_{1,2}\rangle} = P_{|\varphi^{-}_{1,2}\rangle}$ at $J = 0$. Along the charging transition towards the $Q = 1$ sector, the population $P_{|0,5/2\rangle}$ drops quickly to zero. The depletion cycle $t \in [2,\ 4]$ ns simultaneously activates the states $|\varphi_{0,5/2}\rangle$ and $|\varphi_{0,3/2}\rangle$, the stationary regime being described by the RDO $\rho = (|\varphi_{0,5/2}\rangle\langle\varphi_{0,5/2}| + |\varphi_{0,3/2}\rangle\langle\varphi_{0,3/2}|)/2$. Therefore one can use the NF configuration to prepare an equally weighted mixture of states. Along the first depletion sequence, in the NF configuration, $\langle S^{t}_{z}\rangle = 2$ (see figure 4(a)).

In the AP configuration, the first turnstile cycle drives the SMM out of the ground state $|\varphi_{0,5/2}\rangle$ directly into the first excited 'empty' molecular state $|\varphi_{0,3/2}\rangle$ (see figure 3(c)), with no further mixing as in NF configuration. The population of this excited state attains its maximum value within the depletion cycle. In the AP configuration the two EMSs can be viewed as binary digits (i.e. $|\varphi_{0,5/2}\rangle \rightarrow |0\rangle$ and $|\varphi_{0,3/2}\rangle \rightarrow |1\rangle$) that are switched along the turnstile protocol.

The writing of a single EMS depends crucially on the spin polarization of the leads. Figure 3(c) indicates that the 'backward' processes (both charging and relaxation) are forbidden, as the state $|\varphi_{1,3}\rangle$ is not available along the charging sequence because the left lead provides no spin-up electrons. For the same reason there are no

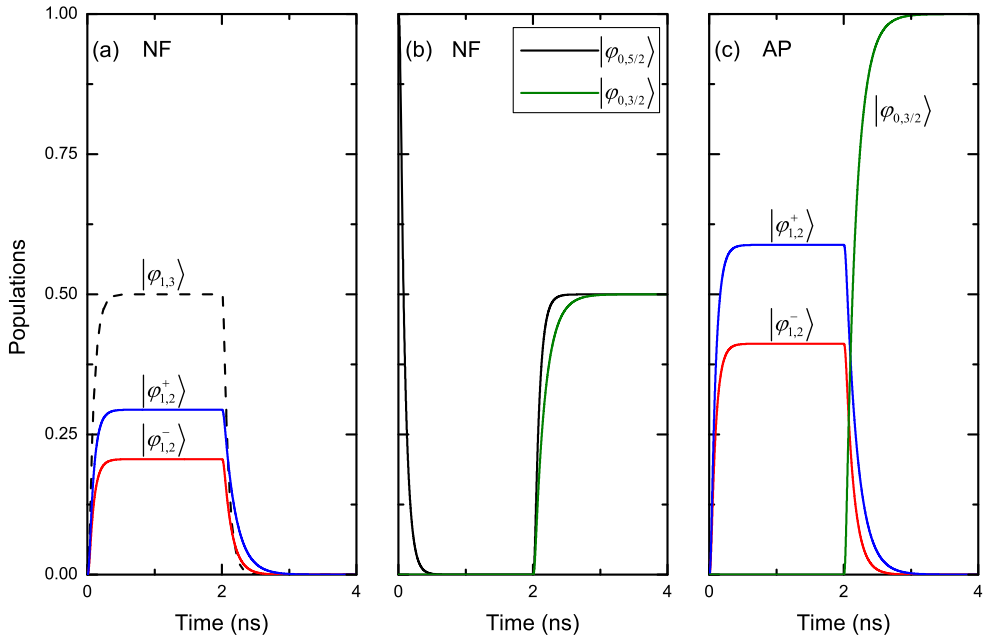

Figure 3. The evolution of the relevant populations along the first turnstile cycle for NF an AP configurations. The charging sequence corresponds to $t \in [0,\ 2]$ ns and the depletion sequence to $t \in [2,\ 4]$ ns. (a) and (b) Normal-ferromagnetic (NF) configuration, (c) antiparallel (AP) configuration; the system ends up in a single excited state $|\varphi_{0,3/2}\rangle$ (see also the discussion in the text). Other parameters: $\epsilon = 0.25$ meV, $J = 0.1$ meV, $U = 1$ meV, $\mu_L = 1$ meV, $\mu_R = -1$ meV, $D = 0.04$ meV, $g\mu_B B = 0.005$ meV and $E/D = 1/250$.

transitions from $|\varphi^{\pm}_{1,2}\rangle$ back to $|\varphi_{0,5/2}\rangle$ on the discharging sequence. In fact, on the charging cycle the system occupies only two states with imbalanced populations $P_{|\varphi^{+}_{1,2}\rangle} > P_{|\varphi^{-}_{1,2}\rangle}$ and which eventually deplete in favor of $|\varphi_{0,3/2}\rangle$. It is important to observe that on the depletion cycle the average total spin $\langle S^t_z\rangle = 3/2$ and coincides with the molecular spin of the $|\varphi_{0,3/2}\rangle$ EMS (see figure 4(a)).

The reverse magnetic switching can be also implemented by simply reversing the bias ($\mu_L \leftrightarrow \mu_R$) while keeping both contacts closed and then repeating the turnstile operation with the new initial state $|\varphi_{0,3/2}\rangle$. Then the system returns to $|\varphi_{0,5/2}\rangle$. This is a *classical* NOT operation, as the system evolves from $|\varphi_{0,5/2}\rangle$ to $|\varphi_{0,3/2}\rangle$ and then back to $|\varphi_{0,5/2}\rangle$ without passing through a superposition of these states.

Let us emphasize that the preparation of a pure excited molecular state $|\varphi_{0,m}\rangle$ cannot be achieved in the standard transport regime. In that case the charge flows simultaneously to and from the leads and one cannot completely deplete the molecule and therefore $\langle\varphi_{0,m}|\rho(t)|\varphi_{0,m}\rangle < 1$. It should be mentioned that for larger S the time needed to achieve the full magnetic switching $m = S \to -S$ also increases as the system must visit all the intermediate states [26]. This fact suggests that the pair of consecutive states ($|\varphi_{0,S}\rangle$, $|\varphi_{0,S-1}\rangle$) might be more appropriate for faster manipulation of magnetic qubits.

Given these results one can ask about the time evolution of the total spin under repeated pumping cycles and on the possibility to read the states prepared along the turnstile operation by measuring currents. Figure 4 summarizes our main results on transient currents and spin evolution along few turnstile cycles for the AP and NF configurations. The time-dependent occupation of the molecular orbital (the blue line in figure 4(a)) has a typical charging/relaxation pattern, with quick orbital filling and slightly slower depletion. This can be seen by comparing the abrupt increase (in less than 1/2 ns) of the population at the beginning of the charging cycles (e.g. $t = 4, 8, 12$ ns) to the smooth tail of discharging which extends over 1 ns (e.g the time range $[6, 7]$ ns).

The total spin average $\langle S^t_z\rangle$ presented in figure 4(a) displays a step-like structure in both configurations. The steps scan both integer and half-integer values of $\langle S^t_z\rangle$, the last step for the AP configuration corresponding to $\langle S^t_z\rangle = 3$ being reached after $t \simeq 18$ ns (not shown). In the AP configuration the onset of half-integer steps corresponds to the depletion of the molecular orbital ($Q = 1 \to Q = 0$), whereas the transition between half-integer to integer steps is associated to the charging process ($Q = 0 \to Q = 1$).

The NF configuration presents different features: there are fewer but longer steps of $\langle S^t_z\rangle$, but no clear correspondence can be made between these steps and the behavior of the total charge Q. One notices that in this case the integer steps extend on some charging sequences and that half-integer values are encountered even if the orbital is empty. Figure 4(b) displays the expected series of spikes for the transient currents $J_{L,R}$ in the AP

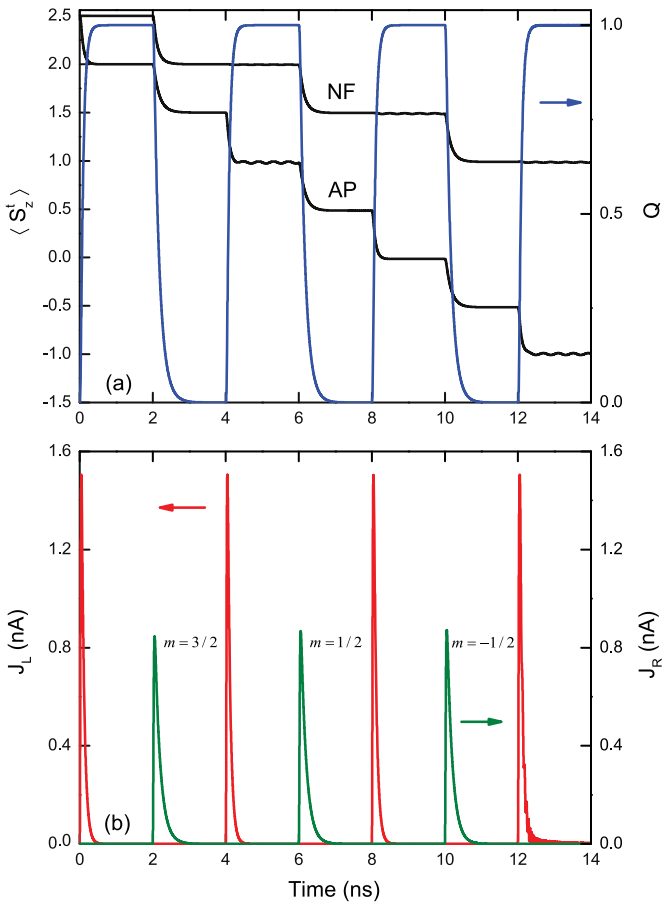

Figure 4. (a) The average total molecular spin $\langle S_z^t \rangle$ in the anti-parallel (AP) and normal-ferromagnetic (NF) configurations (black lines). The step-like structure is discussed in the text. The total charge Q accumulated on the molecular orbital (blue line). (b) The transient currents $J_{L,R}$ in the AP configuration. The half-integer steps of $\langle S_z^t \rangle$ suggest that in the corresponding time range the SMM state is simply $|0,\ m\rangle$; see the discussion in the text. The pumping period is 2 ns. Other parameters: $\mu_L = 1$ meV, $\mu_R = -1$ meV, $\epsilon = 0.25$ meV, $J = 0.1$ meV, $U = 1$ meV and $\tau = 0.5$ meV, $D = 0.04$ meV, $E/D = 1/250$, $g\mu_B B = 0.005$ meV, $V^L = V^R = 0.045$ meV, $k_B T = 0.001$ meV.

configuration. The period of the pumping cycles must be chosen appropriately in order to ensure full charging and discharging of the molecular orbital (we find the minimal period to be ∼1 ns).

We have found a similar behavior (not shown here) for the transient currents in the NF configuration. The input current J_L vanishes when the orbital is fully occupied ($Q = 1$), whereas on the discharging sequence J_R drops to zero as the orbital depletes. The amplitudes of J_L and J_R are different because the charging process is faster than the depletion (see figure 4(a)). By inspecting figures 4(a) and (b) one observes that in the AP configuration we have a one-to-one correspondence between the average $\langle S_z^t \rangle$ and the peak-to-peak sequence in the transient currents: $\langle S_z^t \rangle$ acquires half-integer values only between a depletion peak and the next charging peak (e.g. for $t \in [2,\ 4]$ ns $\langle S_z^t \rangle = 3/2$), while between a charging peak and the next depletion peak the average spin is an integer. This means that the AP configuration can be used to record experimentally the initialization of a given 'empty' molecular state $|\varphi_{0,m}\rangle$.

To this end it is sufficient to know the initial state of the molecule and to carefully 'count' the transient peaks of J_L and J_R. We need to keep in mind though that figure 4(a) shows the *average* value of the total spin, which does not guarantee that along half-integer steps of $\langle S_z^t \rangle$ the system is in a pure state characterized by the RDO $\rho \sim |0,\ m\rangle\langle 0,\ m|$, especially for larger values of the transverse anisotropy when one expects stronger mixing of states.

3.4. Transverse ansiotropy effects

To further investigate the role of the anisotropy, we calculated the populations $P_{|\varphi_{0,m}\rangle}$ of several 'empty' molecular states $|\varphi_{0,m}\rangle$ for different values of the ratio E/D, at fixed magnetic field. Figure 5(a) confirms that at $E/D = 1/250$ the kth depletion cycle is well described by a single state $|\varphi_{0,m=5/2-k}\rangle$. This proves the stepwise all-electrical writing of EMS (i.e. point (i) in the introduction).

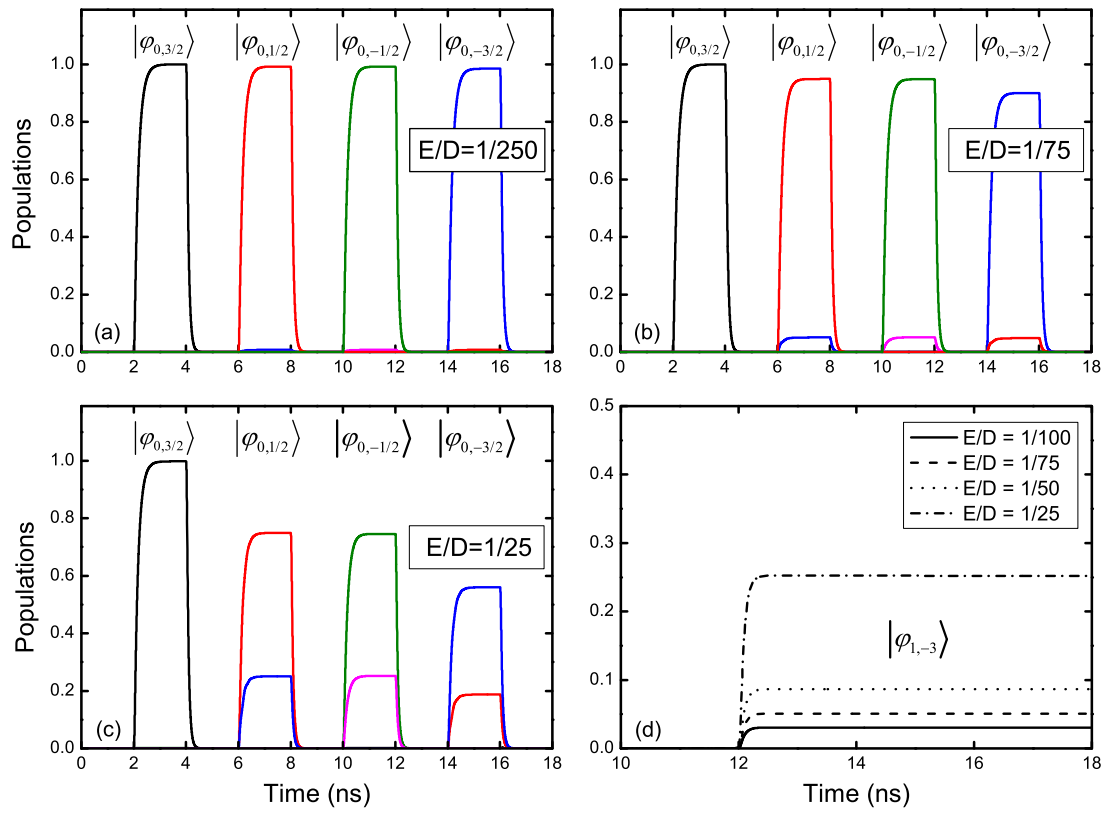

Figure 5. The populations $P_{|\varphi_{0,m}\rangle}$ of the empty molecular states in the antiparallel configuration. Black line: $P_{|\varphi_{0,3/2}\rangle}$, red line: $P_{|\varphi_{0,1/2}\rangle}$, green line: $P_{|\varphi_{0,-1/2}\rangle}$, blue line: $P_{|\varphi_{0,-3/2}\rangle}$, magenta line: $P_{|\varphi_{0,-5/2}\rangle}$. (a) $E/D = 1/250$. (b) $E/D = 1/75$. (c) $E/D = 1/25$. On each turnstile cycle we indicate the dominant EMS. (d) $P_{|\varphi_{1,-3}\rangle}$ for different values of the ratio E/D. The other parameters are the same as those in figure 3.

By increasing the transverse anisotropy constant such that $E/D = 1/75$ we notice in figure 5(b) the emergence of a second EMS on the depletion cycles. Nevertheless, the population of the dominant 'empty' molecular state exceeds 0.9 so we can still associate a well-defined molecular state to *each* of the depletion cycles. This no longer holds for $E/D = 1/25$. Figure 5(c) reveals that the weight of the state $|\varphi_{0,-3/2}\rangle$ and $|\varphi_{0,-5/2}\rangle$ on the second and third depletion cycle increases up to 0.25, reducing the efficiency of the quantum turnstile protocol. Moreover, one can easily see that along the fourth cycle (i.e $t \in [14, 16]$ ns) $P_{|\varphi_{0,-3/2}\rangle} + P_{|\varphi_{0,1/2}\rangle} < 1$ which suggests that other states have to be populated. We have found that the state $|\varphi_{1,-3}\rangle$, corresponding to $Q = 1$ gets populated after the third cycle due to the forward transition $|\varphi_{0,-5/2}\rangle \rightarrow |\varphi_{1,-3}\rangle$ via spin–$\downarrow$ tunneling into the SMM.

In figure 5(d) we show that the population of this state becomes relevant with increasing the anisotropy, i.e. from a population of 0.03 at $E/D = 1/100$ to 0.25 at $E/D = 1/25$.

In order to explain the coexistence of two EMSs on the same depletion sequence when the transverse anisotropy increases we have to analyze the QTM between nearly degenerate $Q = 1$ states. By looking at the off-diagonal matrix element ${}^{\pm}\langle 1, 1|(\hat{S}_+^2 + \hat{S}_-^2)|1, -1\rangle^{\pm}$ we infer that by increasing E the hybridization of $|1, 1\rangle^{\pm}$ and $|1, -1\rangle^{\pm}$ in the fully interacting states increases as well. We find that the weight of the 'minority' state $|1, -1\rangle^{\pm}$ in $|\varphi_{1,1}^{\pm}\rangle$ increases from $\sim 10^{-2}$ for $E/D = 1/250$ to $\sim 10^{-1}$ for $E/D = 1/25$. The mixing of the states $|1, 2\rangle^{\pm}$ and $|1, -2\rangle^{\pm}$ arises to the second order in E and is still negligible. As a consequence the accuracy of the first turnstile cycle is preserved even for E/D as large as $E/D \simeq 1/25$ and that $P_{|\varphi_{0,3/2}\rangle} \approx 1$. This is confirmed by the results presented in figures 5(a)–(c). In order to recover 'clean' EMSs on each depletion cycle for larger values of E/D one could slightly increase the magnetic field. The latter lifts even more the degeneracy of the states $|1, 1\rangle^{\pm}$ and $|1, -1\rangle^{\pm}$ and reduces therefore their mixing in the presence of E/D.

Figure 6(a) presents the relevant populations of EMSs and $Q = 1$ states on the second turnstile cycle ($t \in [4, 8]$ ns) for two values of the ratio E/D. For simplicity we plot the total population of states corresponding to the same dominant value of spin m. Figures 6(b) and (c) indicate schematically the relevant tunneling processes between states of H_M along the charging and discharging sequences. The states $|\varphi_{1,\pm 1}^{\pm}\rangle$ are simultaneously filled along the charging sequence. On the other hand, the states $|\varphi_{1,-1}^{\pm}\rangle$ are less responsive to

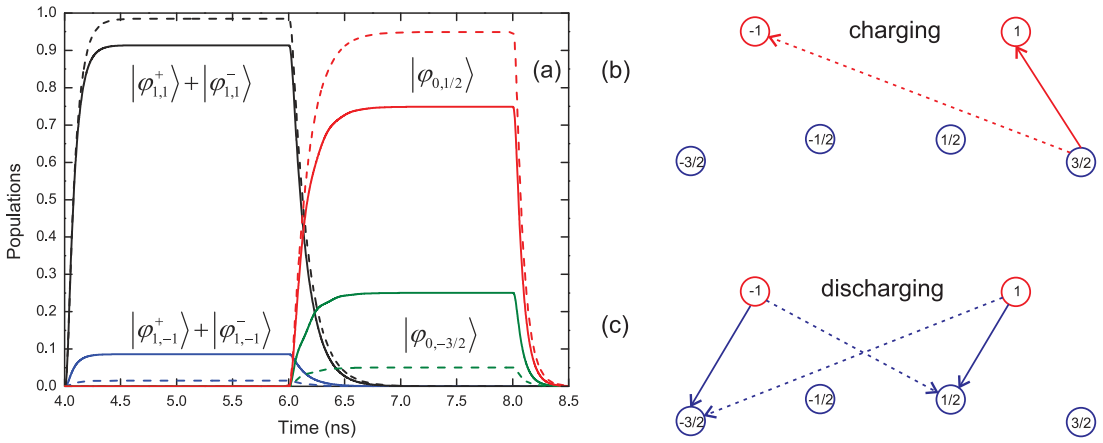

Figure 6. (a) The populations of active states along the second turnstile cycle for two values of the anisotropy constant. The dashed lines correspond to $E/D = 1/75$ and the solid lines to an increased value $E/D = 1/25$. More discussion is given in the text. Other parameters are as in figure 3. (b) and (c): Schematic representation of the tunneling processes between the states $|\varphi^{\pm}_{1,\pm 1}\rangle$ and EMSs along the charging and discharging sequences. The numbers denote the dominant total magnetic moment m of the fully interacting one-particle states.

charging (this processes correspond to the dashed line in figure 6(b)) because spin-down tunneling is allowed only through the states $|1,\ 1\rangle^{\pm}$ whose weights are small. By similar arguments, one can see that the discharging process activates two EMSs, namely $|\varphi_{0,1/2}\rangle$ and $|\varphi_{0,-3/2}\rangle$.

Both of these states acquire important weights in the RDO for $E/D \simeq 1/25$ so the average total spin can no longer be associated to a well-defined value of the molecular spin. We therefore conclude that the enhanced QTM between $Q = 1$ states damages the efficiency of the turnstile protocol even if the EMSs involved in transport are not mixed.

Let us note that the possibility to prepare a single EMS is not obvious as an open system is generally described by a mixed state. Our simulations also show that in the quantum turnstile regime one controls the transitions between any pair of intermediate molecular states ($|\varphi_{0,m}\rangle$, $|\varphi_{0,m-1}\rangle$) along a pumping cycle, in contrast to the full magnetic switching which involves only the pair ($|\varphi_{0,S}\rangle$, $|\varphi_{0,-S}\rangle$).

Finally, we mention that if the SMM has an integer spin one cannot expect an accurate turnstile operation because the transverse anisotropy induces strong mixing between quasidegenerate EMSs (e.g. between $|\varphi_{0,1}$ and $|\varphi_{0,-1}$).

4. Conclusions

In the present work we address the transient transport regime and turnstile pumping across a single-molecule magnet coupled to external leads. The time-dependent evolution of the molecular states has been discussed in detail and signatures of the electrically induced magnetic switching on the transient currents were predicted. For ferromagnetic leads with antiparallel spin polarizations the turnstile protocol allows the stepwise writing and reading of excited molecular states.

The evolution of the states along the turnstile operation can be 'read' indirectly from the behavior of the transient currents. More precisely, by recording the charging and discharging currents one can monitor the evolution of the system and identify the regimes where its density matrix is described by a *single* empty molecular state. This is somehow in contrast to the situation when the leads are simply normal metals and where the control of the excited spin states cannot be achieved as the molecular spin is reversed continuously.

We show that the transverse anisotropy leads to the hybridization of nearly degenerate one-particle states which subsequently relax to empty molecular states with different values of the total spin. However, this dephasing effect can be reduced by applying a moderate perpendicular magnetic field.

Another useful application of the turnstile regime that we address here is the possibility to mix several excited spin states (viewed as magnetic qubits) during the discharging cycles when the source electrode is normal and the drain electrode is ferromagnetic. Note that the short rise time of the switching functions used in our simulations is not essential for the turnstile operation and slower switching functions could be in principle selected to achieve a better resolution of the transient peaks. Our predictive simulations clearly emphasize the potential of the molecular turnstiles as promising candidates for molecular spintronics. As a method approach we have used the generalized master equation formalism adapted to the turnstile configuration.

Acknowledgments

VM and IVD acknowledge financial support from PNCDI2 program (grant PN-II-ID-PCE-2011-3-0091) and from grant no. 45 N/2009. VM, IVD and BT acknowledge financial support from ANCS-TUBITAK Bilateral Programme COBIL 603/2013 and 112T619. BT also thanks TUBA for support.

References

[1] Bogani L and Wernsdorfer W 2008 *Nat. Mater.* **7** 179
[2] Sanvito S 2011 *Chem. Soc. Rev.* **40** 3336
[3] Gatteschi D, Sessoli R and Villain J 2006 *Molecular Nanomagnets* (Oxford: Oxford University Press)
[4] Heersche H B, de Groot Z, Folk J A, van der Zant H S J, Romeike C, Wegewijs M R, Zobbi L, Barreca D, Tondello E and Cornia A 2006 *Phys. Rev. Lett.* **96** 206801
[5] Jo M-H, Grose J E, Baheti K, Deshmukh M M, Sokol J J, Rumberger E M, Hendrickson D N, Long J R, Park H and Ralph D C 2006 *Nano. Lett.* **6** 2014
[6] Komeda T, Isshiki H, Liu J, Zhang Y-F, Lorente N, Katoh K, Breedlove B K and Yamashita M 2011 *Nat. Commun.* **2** 217
[7] Otte A F, Ternes M, von Bergmann K, Loth S, Brune H, Lutz C P, Hirjibehedin C F and Heinrich A J 2008 *Nat. Phys.* **4** 847
[8] Loth S, Lutz C and Heinrich A 2010 *New J. Phys.* **12** 125021
[9] Parks J J *et al* 2010 *Science* **328** 1370
[10] Misiorny M, Weymann I and Barnaś J 2011 *Phys. Rev. Lett.* **106** 126602
[11] Hurley A, Baadji N and Sanvito S 2011 *Phys. Rev.* B **84** 115435
[12] Zyazin A S *et al* 2010 *Nano Lett.* **10** 3307
[13] Song H, Reed M A and Lee T 2011 *Adv. Mater.* **23** 1583
[14] Martin C A, Din D, van der Zant H S J and van Ruitenbeek J M 2008 *New J. Phys.* **10** 065008
[15] Wiesendanger R 2009 *Mod. Phys. Rev.* **81** 1495
[16] Kumar A, Heimbuch R, Poelsema B and Zandvliet H J W 2012 *J. Phys.: Cond. Matter* **24** 082201
[17] Sotthewes K, Heimbuch R and Zandvliet H J W 2013 *J. Chem. Phys.* **139** 214709
[18] Ballmann S and Weber H B 2012 *New J. Phys.* **14** 123028
[19] Kockmann D, Poelsema B and Zandvliet H J W 2009 *Nano Lett.* **3** 1147
[20] Urdampilleta M, Cleuziou J-P, Klyatskaya S, Ruben M and Wernsdorfer W 2011 *Nat. Mater.* **10** 502
[21] Ganzhorn M, Klyatskaya S, Ruben M and Wernsdorfer M 2013 *Nat. Nanotechnol.* **8** 165
[22] Vincent R, Klyatskaya S, Ruben M, Wernsdorfer W and Balestro F 2012 *Nature* **488** 357
[23] Thiele S, Balestro F, Ballou R, Klyatskaya S, Ruben M and Wernsdorfer M 2014 *Science* **344** 1135
[24] Kouwenhoven L P, Johnson A T, van der Vaart N C, Harmans C J P M and Foxon C T 1991 *Phys. Rev. Lett.* **67** 1626
[25] Giblin S P, Wright S J, Fletcher J D, Kataoka M, Pepper M, Janssen T J B M, Ritchie D A, Nicoll C A, Anderson D and Jones G A C 2010 *New J. Phys.* **12** 073013
[26] Timm C and Elste F 2006 *Phys. Rev.* B **73** 235304
Elste F and Timm C 2006 *Phys. Rev.* B **73** 235305
[27] Misiorny M and Barnaś J 2007 *Phys. Rev.* B **76** 054448
Misiorny M and Barnaś J 2007 *Phys. Rev.* B **75** 134425
[28] Timm C and di Ventra M 2012 *Phys. Rev.* B **86** 104427
[29] Wang Rui-Qiang Sheng L, Shen R, Wang B and Xing D Y 2010 *Phys. Rev. Lett.* **105** 057202
[30] Misiorny M and Barnaś J 2013 *Phys. Rev. Lett.* **111** 046603
Misiorny M and Weymann I 2014 *Phys. Rev.* B **90** 235409
[31] Renani F R and Kirczenow G 2013 *Phys. Rev.* B **87** 121403(R)
[32] Barraza-Lopez S, Park K, Garcia-Suarez V and Ferrer J 2009 *Phys. Rev. Lett.* **102** 246801
[33] Chiesa A, Carretta S, Santini P, Amoretti G and Pavarini E 2013 *Phys. Rev. Lett.* **110** 157204
[34] Moldoveanu V, Manolescu A and Gudmundsson V 2009 *New J. Phys.* **11** 073019
[35] Moldoveanu V, Manolescu A, Tang C-S and Gudmundsson V 2010 *Phys. Rev.* B **81** 155442
[36] Tejada J, Chudnovsky E M, del Barco E, Hernandez J M and Spiller T P 2001 *Nanotechnology* **12** 181
[37] Caroli C, Combescot R, Noziere P and saint James D 1971 *J. Phys. C: Solid State Phys.* **4** 916
[38] Mannini M *et al* 2010 *Nature* **468** 417
[39] Ardavan A, Rival O, Morton J J L, Blundell S J, Tyryshkin A M, Timco G A and Winpenny R E P 2007 *Phys. Rev. Lett.* **98** 057201
[40] Bahr S, Petukhov K, Mosser V and Wernsdorfer W 2007 *Phys. Rev. Lett.* **99** 147205
[41] Misiorny M and Barnaś J 2008 *Phys. Rev.* B **77** 172414